



ELSEVIER

Contents lists available at ScienceDirect

# Applied Mathematical Modelling

journal homepage: [www.elsevier.com/locate/apm](http://www.elsevier.com/locate/apm)

## Characterizing turbulent flow over 3-D idealized and irregular rough surfaces at low Reynolds number



Kiran Bhaganagar\*, Long Chau

Department of Mechanical Engineering, University of Texas, San Antonio, TX 78249, United States

### ARTICLE INFO

#### Article history:

Received 20 January 2014

Received in revised form 9 February 2015

Accepted 12 February 2015

Available online 4 March 2015

#### Keywords:

Roughness

DNS

Turbulence

Irregular and regular roughness

### ABSTRACT

The focus of this work is to demonstrate that the response of flow over a rough wall is significantly different for idealized and irregular roughness when the spacing between the roughness elements ( $\lambda$ ) is changed for a given height of the roughness ( $h$ ). For this purpose, turbulence flow in a channel with walls covered with idealized and irregular roughness has been simulated where the  $\lambda/h$  has been systematically varied in the range of 3–35. A detailed study of the flow statistics such as mean flow, root mean square of velocity and vorticity fluctuations was performed. For the idealized roughness both the inner and outer layer of the turbulent boundary layer are altered due to surface roughness, whereas, only the inner layer is altered due to an irregular roughness with similar geometrical parameters. Two distinct regimes that are evident for flow over idealized roughness based on streamwise spacing ( $\lambda/h$ ) can be unified using solidity ratio (measure of degree of sparseness) parameter. Irregular roughness exhibits no sensitivity to  $\lambda/h$  parameter, suggesting that instead of solidity ratio, statistical parameters such as skewness and kurtosis of roughness distribution are more important to classify flow over irregular roughness.

© 2015 Elsevier Inc. All rights reserved.

## 1. Introduction

Understanding turbulent flow over rough surfaces has implications in various fields such as coastal flows (flow over ripples, rough-ocean bed), atmospheric flows (urban roughness and pollution problem), physiological flows (flow in arteries with plaques), gas and wind turbines, ship hulls and turbine blades. However, the presence of various geometrical scales of roughness makes it challenging to compare different numerical simulations or laboratory/field experiments. Characterizing turbulent flow over rough surfaces has been one of the fundamental questions being addressed by researchers.

Towards this direction, a wide range of roughness surfaces have been investigated for idealized (periodic and uniform roughness elements) roughness geometries. Perry et al. [1] studied the turbulent boundary layer over a wall roughened by transverse ribs, and proposed to classify the roughness into two types:  $k$ -type (roughness elements are widely spaced to effectively induce momentum exchange between external and near-wall flow) and  $d$ -type (roughness elements are closely spaced making it difficult for external flow to penetrate into this gap). Tani [2] used the  $\lambda/h$  criterion to demarcate regularly spaced ribs into  $k$  and  $d$  type. From our current understanding of turbulent flow over rough-surfaces it is very clear that  $k$  and  $d$  classification is not a robust and reliable measure of the effect of roughness on the flow, but still the  $\lambda/h$  parameter

\* Corresponding author.

E-mail address: [Kiran.bhaganagar@utsa.edu](mailto:Kiran.bhaganagar@utsa.edu) (K. Bhaganagar).

continues to be one of the pertinent parameters to characterize rough-walls with idealized roughness elements. For 2-D transverse rods, the experiments of [3] for  $\lambda/h = 4$ , direct numerical simulations (DNS) of Leonardi et al. [4] for  $1.3 < \lambda/h < 20$ , the experiments of [5] for  $8 < \lambda/h < 16$ , have demonstrated significant differences in the wall-region as well as the nature of the inner/outer interactions for different  $\lambda/h$ . For 3-D roughness elements, Orlandi and Leonardi [6] and [7] to name a few, have observed the effect of  $\lambda/h$  on near-wall as well as inner/outer interactions.

Recently, there has been significant amount of work on irregular rough surfaces. [8] introduced a geometric parameter, the effective slope of the wall corrugations, showing its ability to characterize the behavior of irregular rough walls, which was confirmed by Flack and Schultz [9] for closely packed pyramids. Subramanian et al. [10] have shown that for rough plate with irregular roughness that resemble turbine blades there was no outer layer effects. Most of the current numerical and experimental works on irregular roughness have focused only on random height and not in the distribution.

Our current interest is to understand the differences in the inner/outer interactions for idealized and irregular roughness. We focus on ripple-shaped roughness elements. The reason is two folds: (a) both idealized and irregular ripple-shaped roughness elements are commonly observed in the bedforms for rough ocean beds, and, (b) we can systematically control the  $\lambda/h$  for the idealized and randomized distribution. To date, to our knowledge, there is no clear consensus on the sensitivity of  $\lambda/h$  on the flow for ripple-shaped roughness.

Direct numerical simulation for turbulent flow in a channel with rough-walls developed by Bhaganagar et al. [11] and well validated for 3-D ripple surfaces by Bhaganagar et al. [12–15] is used as a tool to simulate flow in a channel with rough-walls. In Section 2 we discuss the methodology for generating idealized and random surface and the details of the simulation. We have also included the details of DNS methodology and simulation parameters for completeness. The results are presented in Section 3 and the conclusions are presented in Section 4.

## 2. DNS methodology

The incompressible Newtonian fluid is solved using the fourth-order vertical velocity–vertical vorticity equation as follows:

$$\begin{aligned} \frac{\partial \omega_y}{\partial t} &= H_\omega + \frac{1}{\text{Re}} \nabla^2 \omega_z, \\ \frac{\partial \nabla^2 v}{\partial t} &= H_v + \frac{1}{\text{Re}} \nabla^4 v, \\ v(\pm 1) &= \frac{\partial v}{\partial z}(\pm 1) = 0, \\ \omega_y(\pm 1) &= 0, \end{aligned} \quad (1)$$

where

$$\begin{aligned} H_v &= -\frac{\partial}{\partial z} \left[ \frac{\partial H_1}{\partial x} + \frac{\partial H_2}{\partial y} \right] + \left[ \frac{\partial^2}{\partial x^2} + \frac{\partial^2}{\partial y^2} \right] H_3, \\ H_\omega &= \frac{\partial H_1}{\partial x}. \end{aligned}$$

In this study we define  $(x_1, x_2, x_3) = (x, y, z)$  the streamwise, wall-normal and spanwise coordinates respectively,  $((u_1, u_2, u_3) = (u, v, w))$  are the respective components of velocity and  $(\omega_x, \omega_y, \omega_z)$  are the respective components of vorticity. It is computationally efficient to split the fourth-order equation for  $v$  into two second-order equations and solve the resulting system [16].

In the horizontal directions, the spatial discretizations are done using Fourier series expansion assuming periodicity, and in the wall-normal  $y$  direction the flow is inhomogenous, and the roughness needs to be well resolved. Hence high resolution compact finite differences with spectral-like resolution have been used to obtain the spatial derivatives.

The roughness elements are introduced into the domain using a direct forcing immersed boundary method (IBM) [17] so that the simplicity and efficiency of computation in a Cartesian system is retained. Refer to Bhaganagar et al. [11] for further details on the numerical formulation and validation of the numerical tool. This method gives flexibility in choosing the immersed boundary not found in some other methods, since there is no need to line up the boundary with a grid.

DNS has been performed for a steady flow over rough surface in channel geometry. The streamwise and spanwise domain is  $12.56\delta$  and  $4.18\delta$  respectively, where  $\delta$  is the half height of the channel. The upper surface of the channel is flat (we refer to as the smooth-side) and the random rough elements are imposed on the lower surface. The roughness elements have a height from crest to trough of  $0.12\delta$ . In the wall-normal direction, non-uniform mesh was used. The grid spacing varied from 0.94 wall-units adjacent to the virtual no-slip surface to 6.5 wall-units at the centerline. In the horizontal directions, the streamwise and spanwise grid spacing was approximately 15 and 8 wall-units respectively.

The spatial discretization used 256 streamwise Fourier modes, 257 wall-normal compact finite-difference grid points of fourth-order accuracy and 256 spanwise Fourier modes. Turbulent initial conditions were imposed for the entire computational domain and the simulations were performed for sufficiently long time (100 non-dimensional time units based on channel half height and  $u_\tau$ ) until converged statistics were obtained. Simulations were performed on a parallel super-computing cluster consisting of one-hundred and twenty-eight nodes with wall-clock time of 2 days. The mean statistics

were obtained from streamwise and spanwise averaging for at least 100 non-dimensional time units. The DNS code has been thoroughly validated for channel with rough-walls consisting of three-dimensional egg-pattern roughness elements [14] and for 2-D and 3-D wavy roughness [11]. The spatial and temporal resolution, grid convergence, turbulence statistics have been validated.

To understand the effect of the roughness geometry on turbulent flow, organized patterns of three dimensional roughness elements are considered first. The idealized roughness elements have been generated to mimic the three dimensional ripple shaped bedforms found on the ocean floor. The geometry chosen is different from previous studies in the fact that it accounts for variation of profile geometry in three dimensions, whereas the majority of previous studies have focused on flow over two dimensional ripples/bedforms. Ripples with periodic behavior in two directions have been observed in nature and have been experimentally created by Andersen and Faraci, who observed that serpentine shaped ripples formed when the ratio of

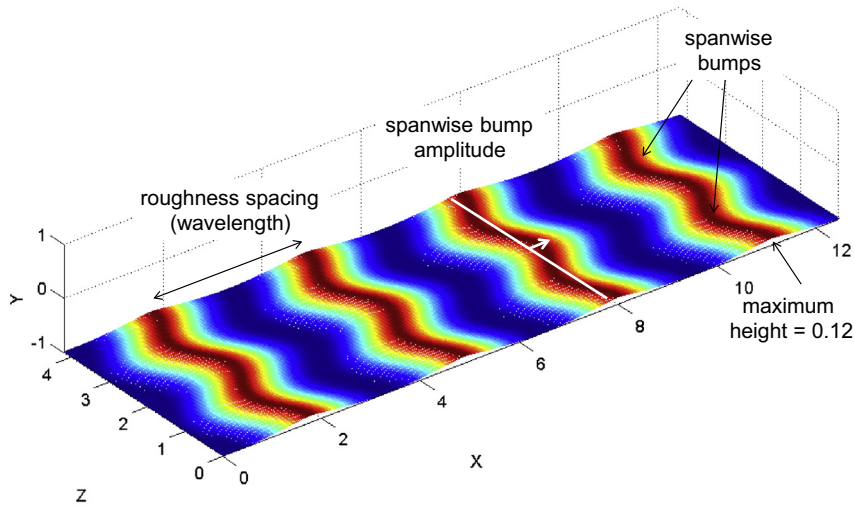


Fig. 1. Three-dimensional idealized serpentine roughness generated using Eq. (1) with the following parameters  $h = 0.12$ ,  $A = 1$ ,  $B = A/5$  and  $C = 3$ .

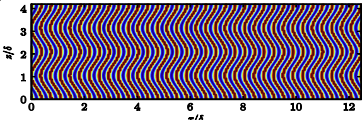
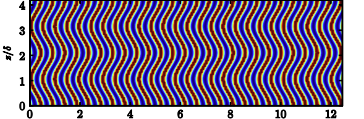
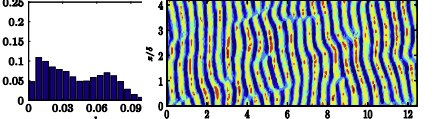
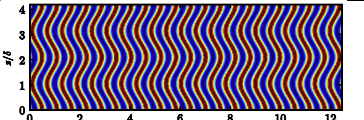
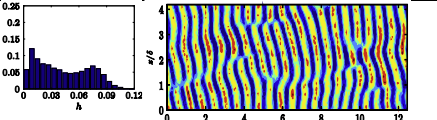
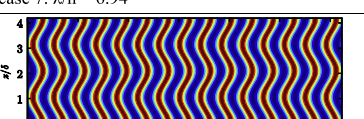
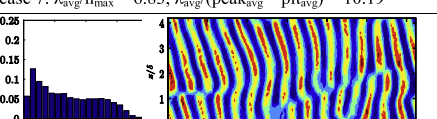
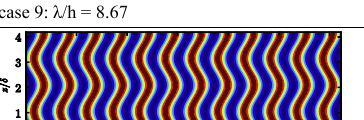
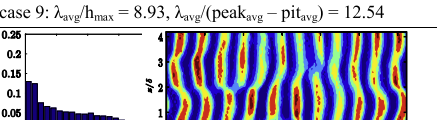
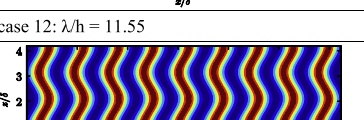
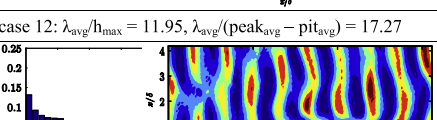
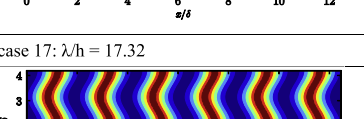
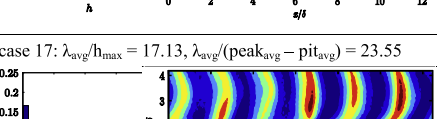

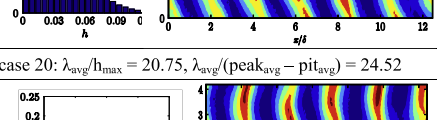
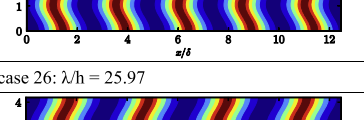
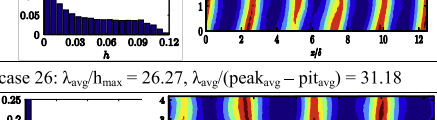
Table 1  
Statistical parameters for ideal roughness surfaces.

Case	$\lambda/h$	$\bar{h}/\delta$	$\sigma/\delta$	rms	$k_s$	$k_k$
3	3.06	0.0466	0.0417	0.0625	0.654	2.094
4	4.00	0.0453	0.0399	0.0604	0.639	2.159
5	4.95	0.0509	0.0418	0.0659	0.365	1.693
7	6.93	0.0488	0.0407	0.0635	0.426	1.781
9	8.67	0.0525	0.0421	0.0672	0.279	1.582
12	11.56	0.0502	0.0413	0.0650	0.359	1.676
17	17.33	0.0480	0.0402	0.0626	0.429	1.783
20	20.80	0.0472	0.0397	0.0617	0.448	1.819
26	26.00	0.0465	0.0393	0.0608	0.466	1.853
35	34.67	0.0457	0.0388	0.0599	0.481	1.885

Table 2  
Statistical parameters for irregular roughness surfaces.

Case	$\lambda_{avg}/h_{max}$	$\lambda_{avg}/peak_{avg}-pit_{avg}$	$\bar{h}/\delta$	$\sigma/\delta$	rms	$k_s$	$k_k$
4	4.00	6.84	0.0414	0.0263	0.0491	0.322	1.914
5	4.95	7.62	0.0426	0.0280	0.0510	0.285	1.791
7	6.93	10.19	0.0423	0.0287	0.0511	0.409	1.957
9	8.67	12.54	0.0407	0.0309	0.0511	0.498	2.057
12	11.56	17.27	0.0401	0.0297	0.0499	0.527	2.210
17	17.33	23.55	0.0369	0.0296	0.0473	0.583	2.198
20	20.80	24.52	0.0391	0.0332	0.0513	0.591	2.039
26	26.00	31.18	0.0366	0.0335	0.0496	0.679	2.184

**Table 3**  
Streamwise-spanwise plane view of ideal and irregular roughness surfaces.

X-Z view of Idealized Roughness	PDF of roughness height and X-Z view for irregular roughness
case 3: $\lambda/h = 3.06$ 	
case 4: $\lambda/h = 4.02$ 	case 4: $\lambda_{avg}/h_{max} = 4.12, \lambda_{avg}/(peak_{avg} - pit_{avg}) = 6.84$ 
case 5: $\lambda/h = 4.98$ 	case 5: $\lambda_{avg}/h_{max} = 4.91, \lambda_{avg}/(peak_{avg} - pit_{avg}) = 7.62$ 
case 7: $\lambda/h = 6.94$ 	case 7: $\lambda_{avg}/h_{max} = 6.83, \lambda_{avg}/(peak_{avg} - pit_{avg}) = 10.19$ 
case 9: $\lambda/h = 8.67$ 	case 9: $\lambda_{avg}/h_{max} = 8.93, \lambda_{avg}/(peak_{avg} - pit_{avg}) = 12.54$ 
case 12: $\lambda/h = 11.55$ 	case 12: $\lambda_{avg}/h_{max} = 11.95, \lambda_{avg}/(peak_{avg} - pit_{avg}) = 17.27$ 
case 17: $\lambda/h = 17.32$ 	case 17: $\lambda_{avg}/h_{max} = 17.13, \lambda_{avg}/(peak_{avg} - pit_{avg}) = 23.55$ 
case 20: $\lambda/h = 20.77$ 	case 20: $\lambda_{avg}/h_{max} = 20.75, \lambda_{avg}/(peak_{avg} - pit_{avg}) = 24.52$ 
case 26: $\lambda/h = 25.97$ 	case 26: $\lambda_{avg}/h_{max} = 26.27, \lambda_{avg}/(peak_{avg} - pit_{avg}) = 31.18$ 

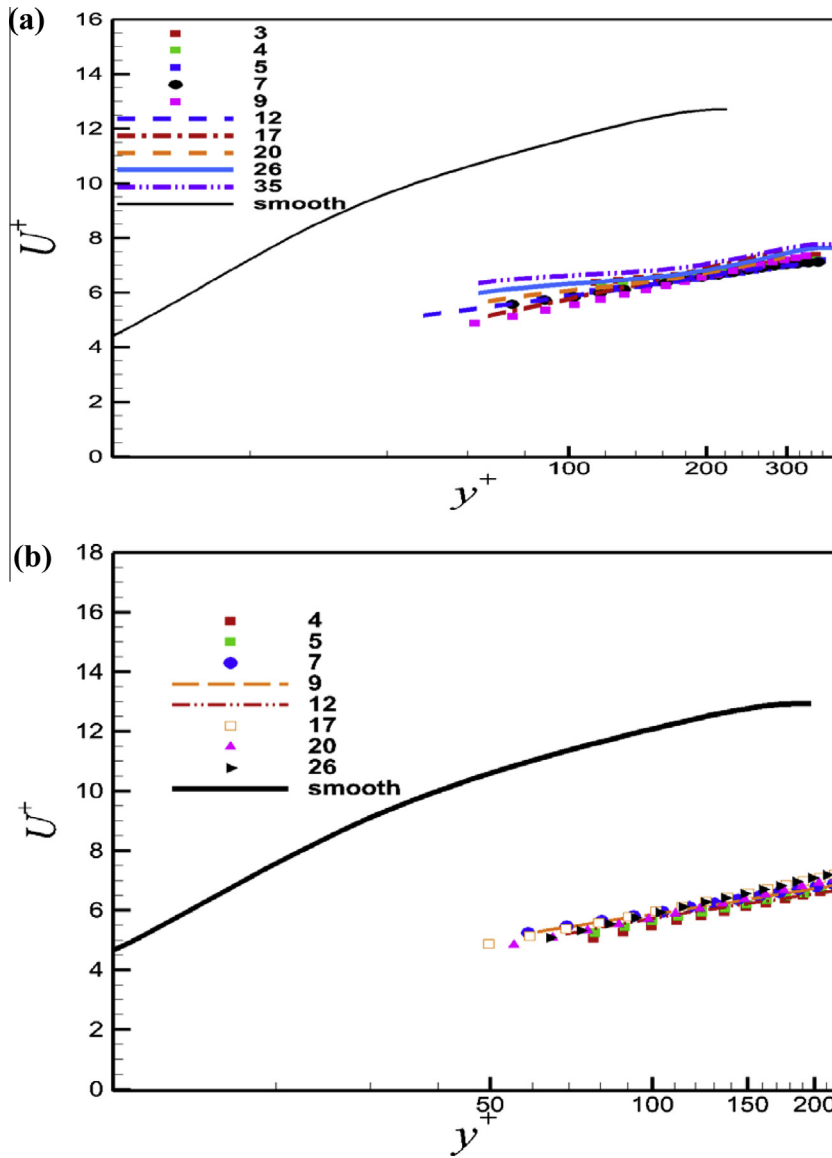


Fig. 2. Mean velocity profile normalized by local (rough-wall)  $u_\tau$  for flow over (a) idealized roughness (b) irregular roughness, plotted in wall units.

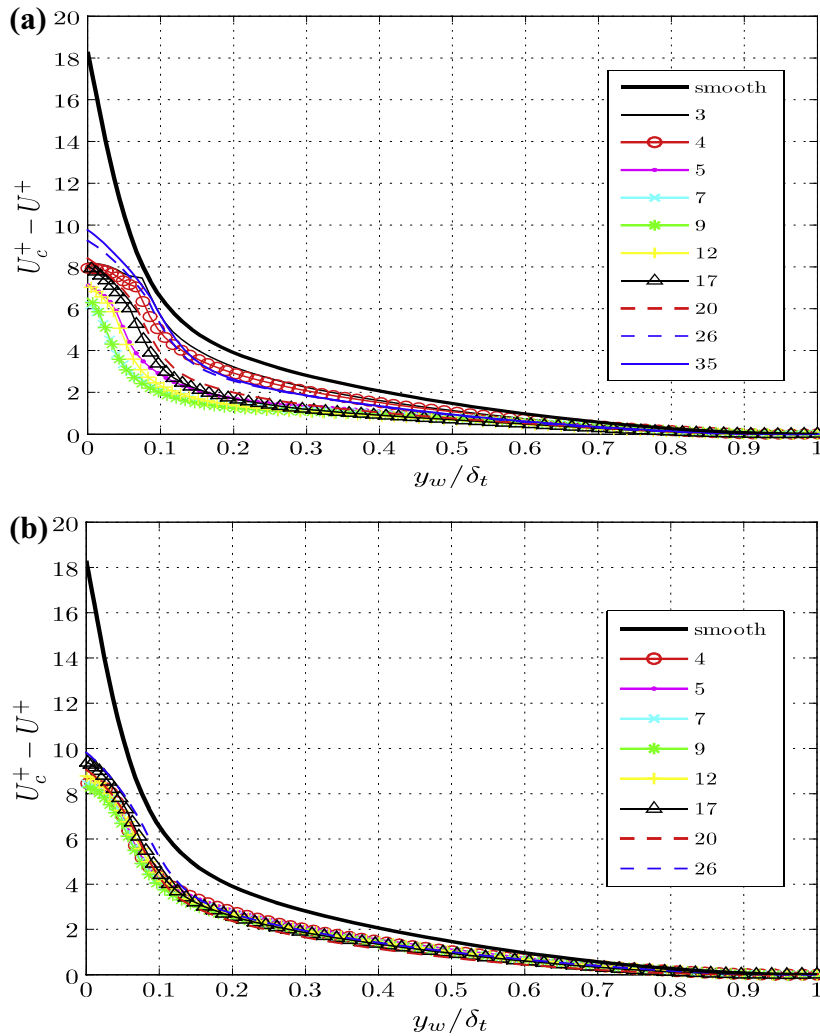
current strength and wave orbital velocity was approximately 0.5. For this purpose, the steep crests that are seen in ripples have been represented in the present study by selecting the ripple profile of the form:

$$y = -h|\cos(Ax - B\cos(Cz))|, \tag{2}$$

where,  $h$  denotes the maximum ripple height scaled with the half-height of the channel ( $\delta$ ),  $A$  is a parameter controlling the streamwise roughness wavelength,  $B$  is a parameter controlling the amplitude of spanwise bumps,  $C$  is a parameter controlling the number of spanwise bumps, and  $x$  and  $z$  are the streamwise and spanwise locations, respectively. The sharp peak of each ripple crest was then smoothed out slightly using a spline interpolation between neighboring points of the crest. An example of the channel geometry with idealized roughness is shown in Fig. 1.

The irregular surfaces have been created using a model for sand ripples [18] and Nishimori and Ouchi. Refer to Chau and Bhaganagar [19] for details. The model is discrete in space and time and begins by assigning a random value between 0 and 1 to each grid point on the computational domain to replicate a rough, but flat, sand bed of height corresponding to the desired maximum height of the roughness.

For this study, ten idealized surfaces and eight irregular surfaces are considered. The calculated parameters for all of the idealized surfaces are shown in Table 1, and the parameters for the irregular surfaces are shown in Table 2. We computed the statistical parameters i.e. the mean ( $\bar{h}$ ), standard deviation ( $\sigma$ ), root-mean-square (rms), skewness ( $k_s$ ) and kurtosis ( $k_k$ ) of



**Fig. 3.** Mean velocity defect profile normalized by local (rough-wall)  $u_\tau$  for flow over (a) idealized roughness (b) irregular roughness, plotted vs. wall distance normalized by apparent half-height of the channel ( $\delta_t$ ).

the roughness height. For the idealized surfaces, the  $\lambda/h$  varies from 3 to 35, and for the irregular surfaces, the  $\lambda/h$  varies from 4 to 26. The maximum roughness height ( $h/\delta$ ) for all the cases is 0.12. The case numbers correspond to the corresponding value of  $\lambda/h$ , e.g. case 3 corresponds to case with  $\lambda/h = 3$ . For the irregular roughness geometry the value of  $\lambda_{avg}/(\text{peak}_{avg} - \text{pit}_{avg})$  has also been computed. The  $x$ - $z$  cross sectional view of the roughness along with the probability density distribution (PDF) of roughness height is presented in Table 3. All 3-D roughness surfaces have fixed two sinusoidal shaped bumps in the spanwise direction. The non-dimensional height of these bumps for all cases is 0.12.

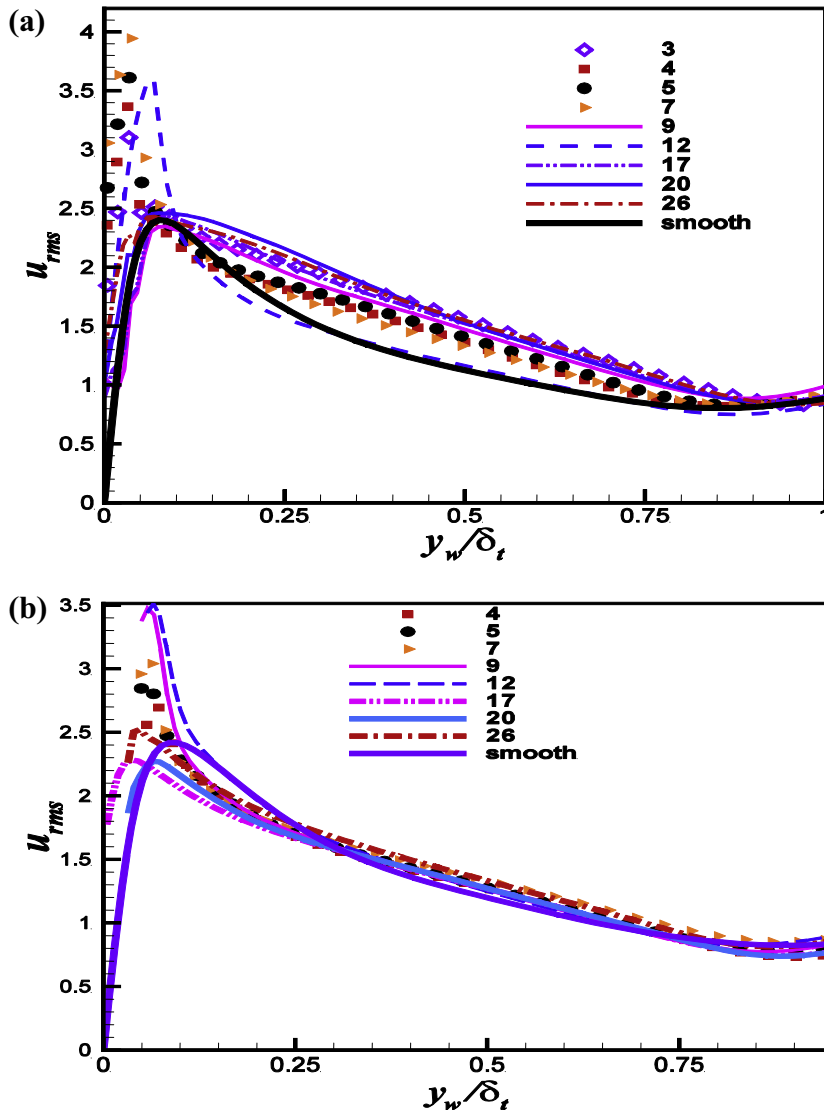
### 3. Results: flow statistics

DNS of flow over idealized and irregular 3-D roughness was performed at Reynolds based on wall-shear stress ( $Re_\tau$ ) = 180 for cases shown in Table 1 and Table 2 respectively. It should be noted that all the time-averaged statistics have been computed by first averaging in the horizontal plane and then long time-averages of these spatially averaged quantities.

#### 3.1. Mean flow

The mean velocity profile is analyzed first. The mean velocity profile over a rough surface can be expressed in terms of the virtual offset  $\alpha$ , roughness length scale  $y_0$  in the following form:

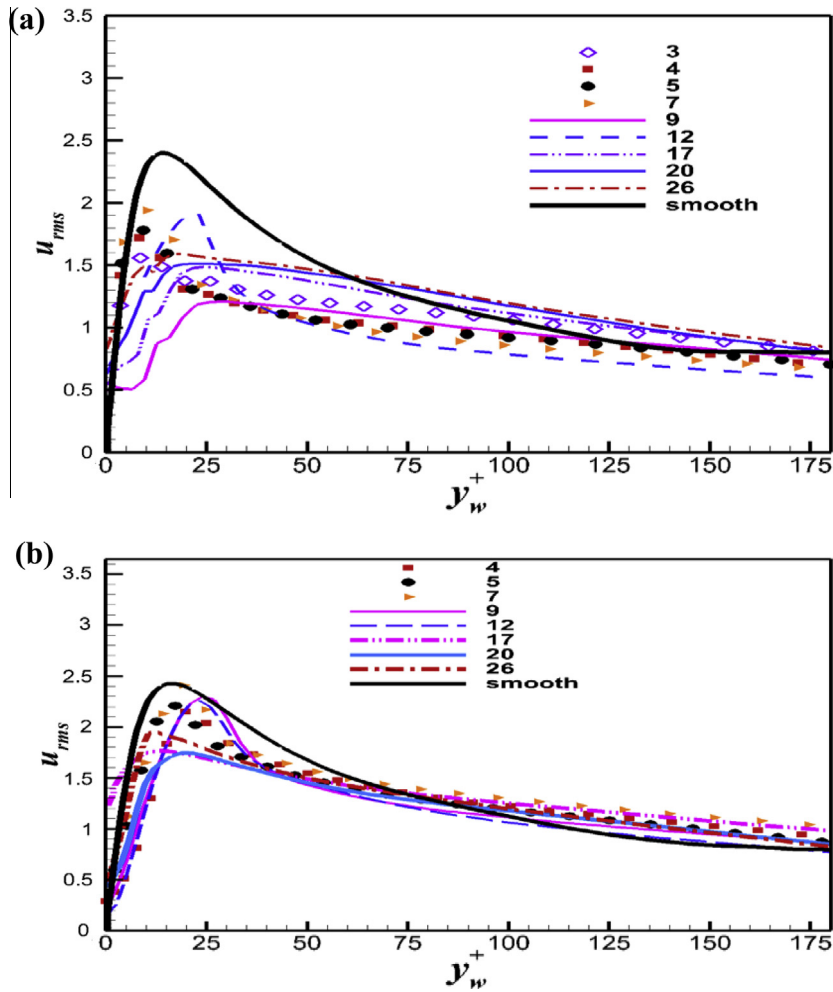
$$\mathbf{U}/u_\tau = \mathbf{1}/\kappa \ln \frac{(\mathbf{y}_w - \alpha)}{y_0}. \quad (3)$$



**Fig. 4.** Turbulent intensity of streamwise velocity component normalized by  $u_{\tau}$  at the smooth wall. The wall-normal distance taking the virtual offset into account is normalized by  $\delta_t$  (distance from the wall to the  $y$  location corresponding to minimum  $u_{rms}$ ) (a) idealized roughness (b) irregular roughness.

Here,  $y_w$  is the distance from the wall. For the smooth-wall case  $u_{\tau}$  is obtained using the shear at the upper smooth wall, and for the rough wall  $u_{\tau}$  is obtained from the mean momentum balance equation. Here,  $\alpha$  and  $y_0$  are determined by fitting the mean velocity in the inertial sublayer using Eq. (2).

The mean velocity profile normalized by local (rough-wall)  $u_{\tau}$  plotted in wall units is shown in Fig. 2. All the results consider the virtual offset at the rough-wall side. In this figure,  $y^+$  represents the distance from the wall in wall units. We compute  $y^+$  taking the virtual offset into account and using the local  $u_{\tau}$ . Roughness produces the expected downward shift in  $U^+$ , for both the idealized and irregular rough walls. For the idealized roughness, downward shift of  $U^+$  varies from 5.6 to 6.06 with a maximum shift at  $\lambda/h = 7$ . Further,  $u_{\tau}$  magnitude increases with decreasing spacing attaining a maximum at  $\lambda/h = 7$ , suggesting that the roughness effects increases with increasing spacing and reaches a peak at  $\lambda/h = 7$ . Beyond this spacing, the trend is reversed and the roughness effect decrease with increasing space. However, for irregular roughness there is no significant effect of spacing on the roughness effects with more or less nearly similar downward shift in the mean velocity. However, the friction velocity has shown a dependence on the spacing, though no particular trend was observed. To see the effects of the spacing on the outer layer of the turbulent boundary layer, the mean-velocity defect normalized by local  $u_{\tau}$  was plotted vs.  $y_w$  normalized by  $\delta_t$ , where  $y_w$  is the distance from the wall and  $\delta_t$  is defined as the distance from the wall to the  $y$  location corresponding to minimum rms velocity fluctuations (figures are not shown). It should be noted that  $\delta_t$  should be used for normalizing to account for the virtual offset at the rough-wall. In the outer layer, the mean-velocity profile in the outer layer is independent of the roughness elements for both the idealized and irregular rough wall turbulent boundary



**Fig. 5.** Turbulent intensity of streamwise component of velocity fluctuation normalized by local  $u_\tau$  plotted in corresponding wall units, shown in near-wall region (a) idealized roughness (b) irregular roughness.

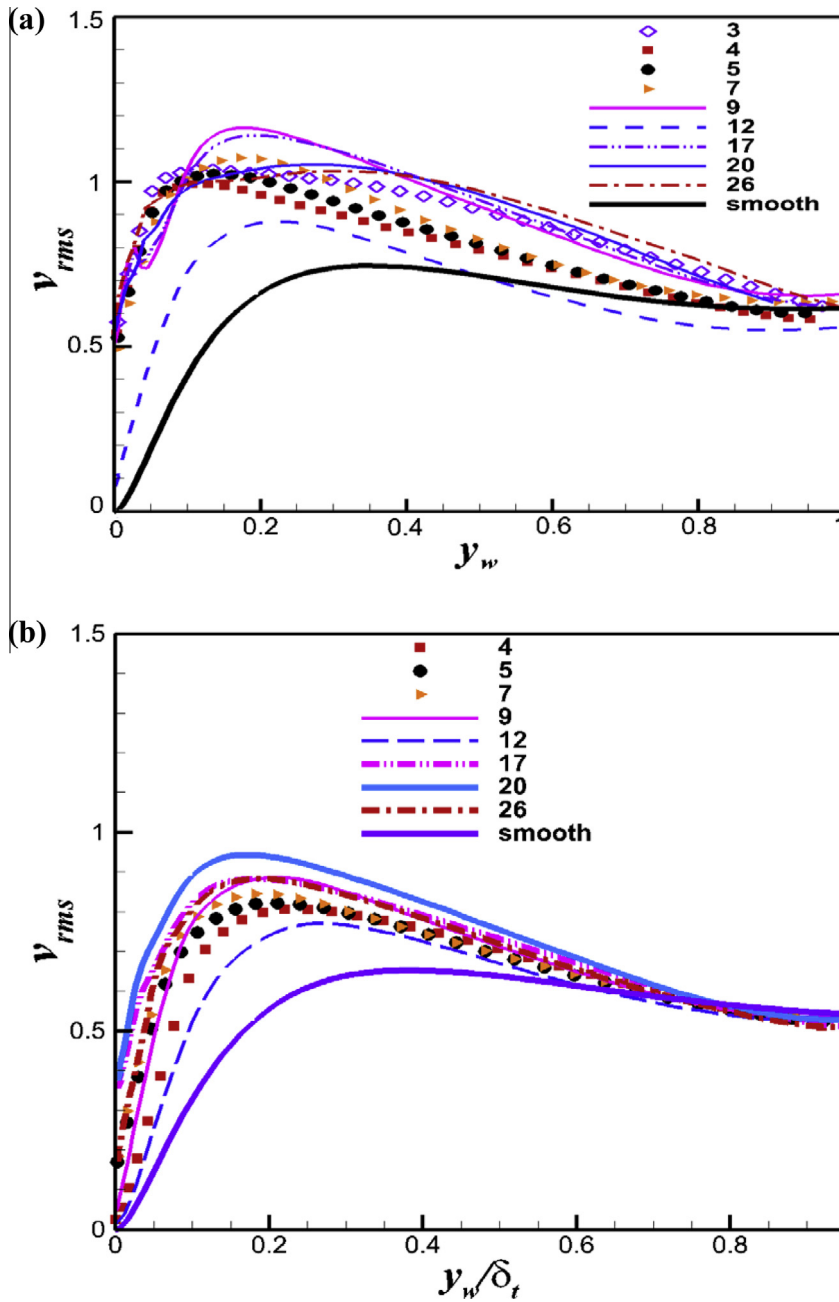
layer. Close to the wall, as expected, there is a strong dependence on  $\lambda/h$  for the idealized roughness; but, the flow is almost insensitive to the spacing parameter for the irregular roughness. The regular 3-D ripple shaped roughness behaves similar to the idealized egg-carton roughness [11], where we demonstrated that the roughness alters the mean flow velocity only in the inner layer, and the outer layer of the mean velocity is unaffected by the presence of surface roughness.

Fig. 3 shows the mean-velocity defect plotted in outer units. Plotted in this manner, the flow over idealized rough wall is sensitive to  $\lambda/h$  in the inner region; whereas the flow over irregular rough wall is almost similar for all cases. The outer-region is not altered due to roughness for both the idealized and irregular rough walls. In conclusion, the mean flow over idealized rough wall is sensitive to  $\lambda/h$ , and two distinct behaviors for the densely and sparsely packed roughness are evident. The mean flow over irregular wall is insensitive to  $\lambda/h$ .

### 3.2. Root-mean-square of velocity and vorticity fluctuations

We next compare the differences in the turbulent intensities for velocity in both the inner and outer layers, between the idealized and irregular rough walls. We examine the root mean square (rms) of velocity fluctuations. Fig. 4(a) and (b) shows the rms of the streamwise velocity fluctuations normalized by smooth wall  $u_\tau$  for the idealized and irregular rough wall cases respectively. The  $u_{rms}$  has been plotted vs. wall-normal distance scaled by  $\delta_r$ , the  $y$  location of the minimum  $u_{rms}$ . The mean velocity results collapse better when scaled by  $\delta_r$ . Further, it should be noted that the present simulations (figures are not shown) have clearly shown that the location of the minimum  $u_{rms}$  shifts to the upper half of the channel for all the cases considered, however, this shift is very sensitive to the spacing as well as the nature of the roughness, i.e. idealized or irregular roughness elements. For the idealized roughness, this shift increases with increasing  $\lambda/h$  for  $\lambda/h < 7$ , and decreases with



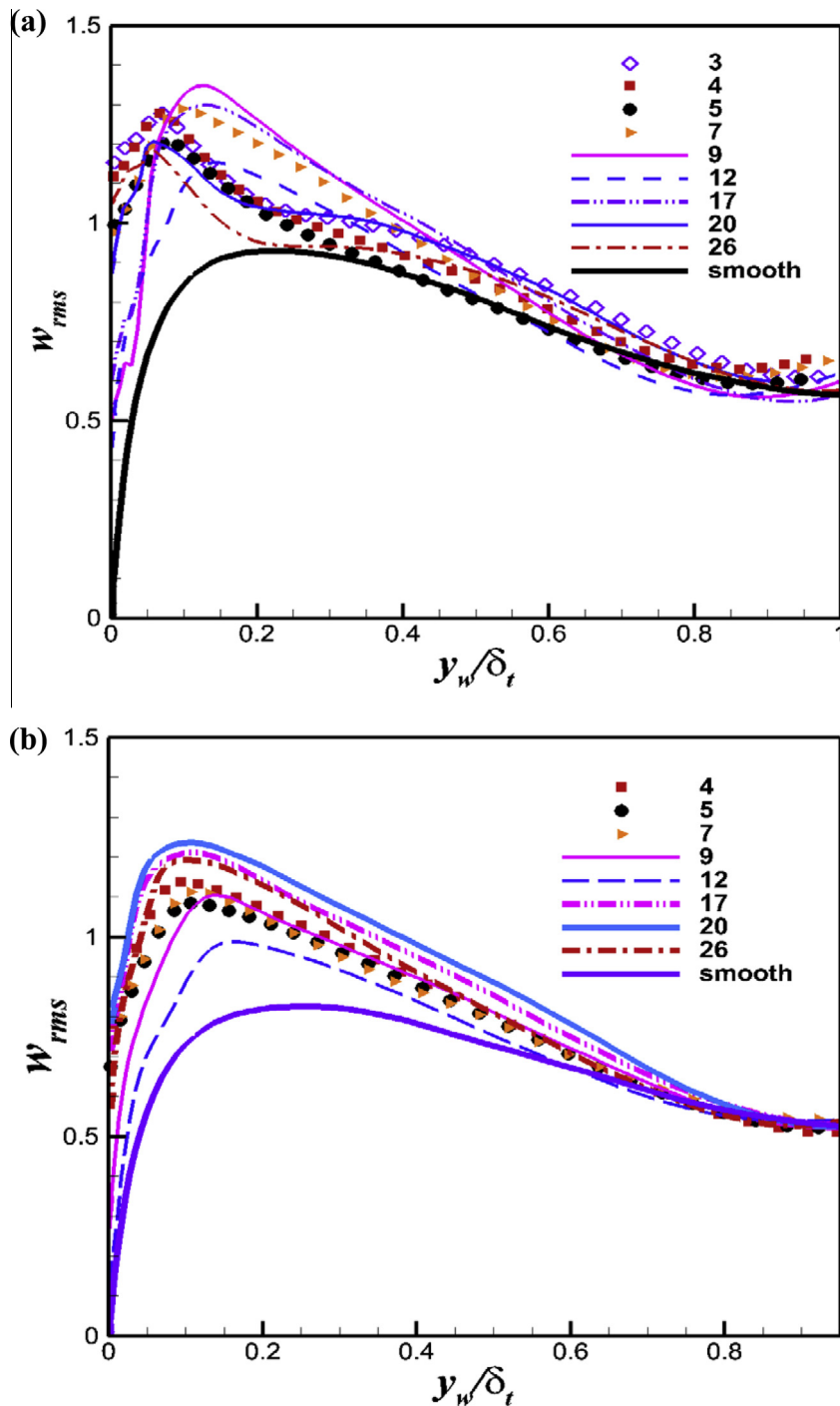


**Fig. 6.** Wall-normal turbulent intensities for flow normalized by smooth wall  $u_\tau$  vs. wall-normal distance normalized by the channel half-height (a) idealized rough wall (b) irregular rough wall.

increasing  $\lambda/h$  for  $\lambda/h > 7$ . Whereas, the shift is independent of  $\lambda/h$  for irregular roughness. It is clear that as the rough wall for different cases has different thickness,  $\delta_t$  is a better scaling measure for the outer layer.

The turbulence intensities over both idealized and irregular rough walls are higher compared to the smooth walls. However, the differences between the idealized and irregular roughness are very striking. The outer layer is altered for rough wall with idealized roughness for all the cases, and moreover, the effect of  $\lambda/h$  is clearly present. For the irregular roughness, the differences between the rough wall and the smooth wall are observed only up to  $y_w/\delta_t = 0.25$ . The effect of roughness is confined only to the inner layer and the outer layer is unaltered for rough wall with irregular roughness elements. To understand the extent of alterations of flow in the inner layer due to roughness, we look into  $u_{rms}$  in inner units.

Fig. 5(a) and (b) shows the  $u_{rms}$  scaled by local  $u_\tau$  plotted in wall units for the idealized and irregular rough-wall cases respectively. The inner layer shows a strong sensitivity to the spacing for all the cases considered. However, the effect of



**Fig. 7.** (a) Spanwise turbulent intensities normalized by smooth wall  $u_\tau$  for (a) idealized rough wall (b) irregular rough wall. Dotted line indicates location of roughness peaks.

spacing extends to a larger wall-normal distance for the idealized rough wall. On the other hand, for irregular roughness, the influence of roughness is present throughout the inner layer, but the flow does not recognize the effect of  $\lambda/h$  beyond 40–45 wall units.

The rms of the wall-normal and spanwise components of velocity are considered next to identify the effect of roughness in the outer layer of the boundary layer. The  $v_{rms}$  normalized by smooth wall  $u_\tau$  plotted vs. wall normal distance scaled by  $\delta_\tau$  is shown in Fig. 6(a) and (b) for idealized roughness and irregular roughness respectively. Differences in  $v_{rms}$  between the

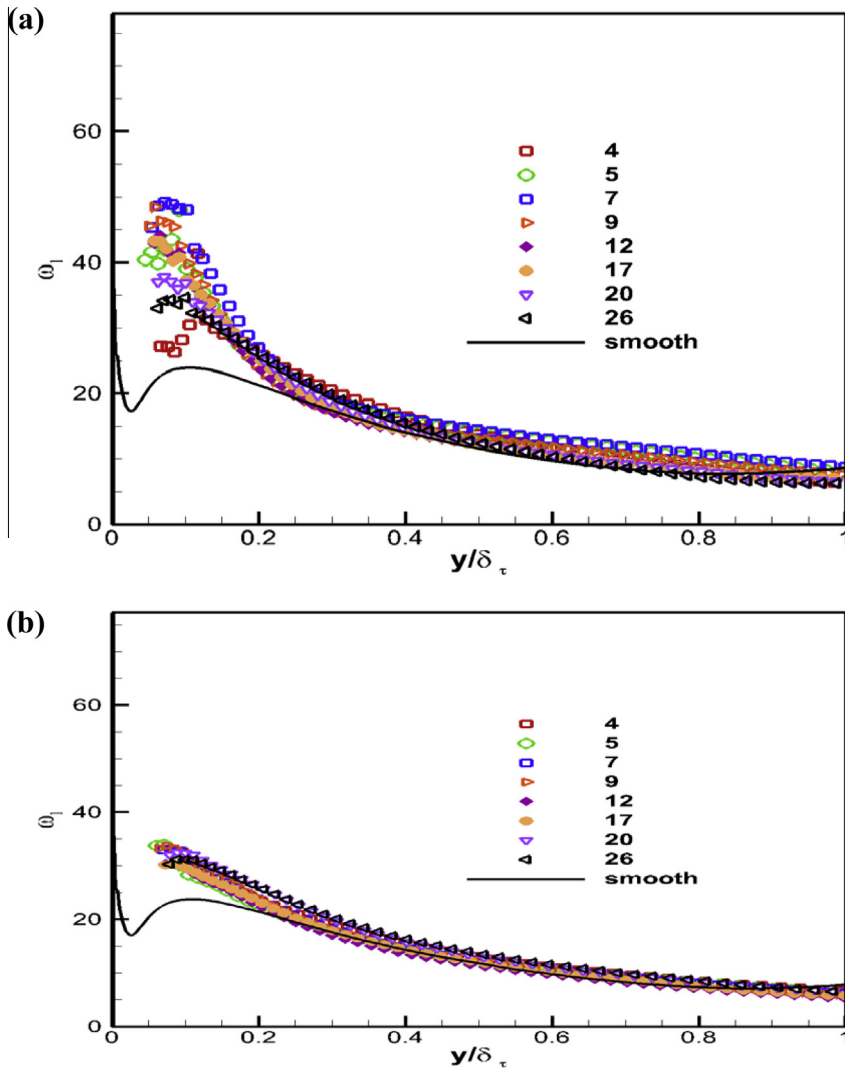


Fig. 8. (a) idealized roughness  $\omega_x$ , (b) irregular roughness  $\omega_x$ , (c) idealized roughness  $\omega_z$ , (d) irregular roughness  $\omega_z$  normalized by smooth wall  $u_\tau$  and  $\delta_\tau$ .

smooth wall and idealized rough wall are present throughout the boundary layer. Further, the effect of spacing is also present in the outer layer of the turbulent boundary layer. It should be noted that for rough wall with idealized roughness, the outer layer is affected due to roughness for all the cases; however, this effect is more profound for  $\lambda/h < 9$ . The outer layer of  $v_{rms}$  is not significantly altered due to roughness for rough wall with irregular roughness.

Fig. 7(a) and (b) show the spanwise turbulent intensity normalized by the smooth wall  $u_\tau$ . Similar to  $u_{rms}$  and  $v_{rms}$ , the  $w_{rms}$  for rough wall with idealized roughness shows a strong sensitivity to spacing both in the inner- and the outer-layers. The outer layer is not altered for rough wall with irregular roughness.

The analysis of turbulence intensities has revealed that the differences between the flow over idealized and irregular roughness of similar roughness are very striking. The turbulence intensities are very sensitive to the effect of  $\lambda/h$  both in the inner and the outer layers for ideal roughness. Further, similar to the mean flow, two distinct regimes are evident for the densely and sparsely spaced roughness. For the irregular roughness, only the inner layer is altered due to roughness, and the effect of  $\lambda/h$  is evident close to the wall. Away from the wall, the turbulence is not altered due to irregular roughness.

We next analyze the rms of the vorticity fluctuations to provide insight into how the small-scale features are altered due to roughness. The results of  $\omega_x$  and  $\omega_z$  normalized using local  $u_\tau$  and  $\delta_\tau$  are presented in Fig. 8. The magnitudes of vorticity fluctuations for rough wall are higher compared to smooth wall for both ideal and irregular rough-walls. The roughness spacing has an effect on  $\omega_x$  in the near-wall region wall for rough wall with idealized roughness (see Fig. 8(a)); irregular roughness alters  $\omega_x$  in the near-wall region; however, the effect of roughness spacing is almost negligible (see Fig. 8(b)). The location of peak  $\omega_x$  changes with  $\lambda/h$  for idealized roughness, whereas the peak location is at the same wall-normal

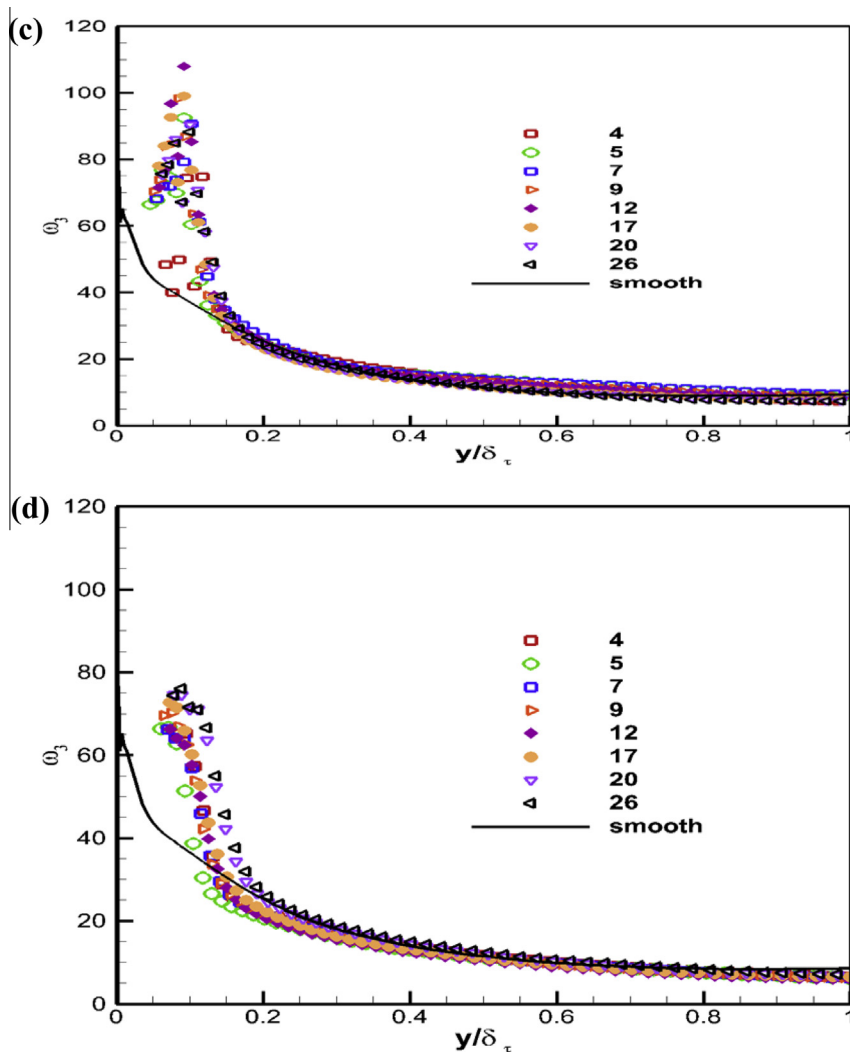


Fig. 8 (continued)

distance as for the smooth wall for irregular roughness. In the outer layer, very small differences exist between the rough wall and smooth wall  $\omega_x$  for both irregular and ideal rough-walls, suggesting that roughness does not alter the outer layer of vorticity fluctuations.

The rms of the spanwise vorticity is altered in the near-wall region for both the ideal and irregular rough-walls; however, the intensity of spanwise vorticity is much higher for the ideal rough-wall than the irregular rough-wall (see Fig. 8(c) and (d) respectively). Close to the wall, differences between the different roughness spacing cases for irregular rough-wall are evident, but these differences are not as dominant as for the ideal rough-wall. In the outer layer, roughness does not alter  $\omega_z$  for both ideal and irregular rough-walls. The results have clearly demonstrated significant differences in the turbulence intensities and in the vorticity fluctuations between the idealized and irregular roughness cases. Finally, we consider the differences in the total stress distribution.

### 3.3. Shear stress

Shear stress distributions are shown in Fig. 9 ( $\lambda/h = 9$  is chosen as an example). The flow has reached an equilibrium state, indicated by the linear profile of the total stress ( $-\mathbf{u}'\mathbf{v}' + \frac{1}{Re} \frac{\partial \bar{u}}{\partial y}$ ). Significant differences between the idealized and irregular roughness cases are clearly evident. The total shear on the rough wall side for idealized case is much higher compared to the irregular roughness case, suggesting enhanced friction factor for idealized roughness. The Reynolds stress near the rough wall is much higher for the idealized case compared to the irregular roughness case; on the other hand, the viscous stress is roughly of the same magnitude. To understand the trend over different spacing, the maximum values of total shear stress,

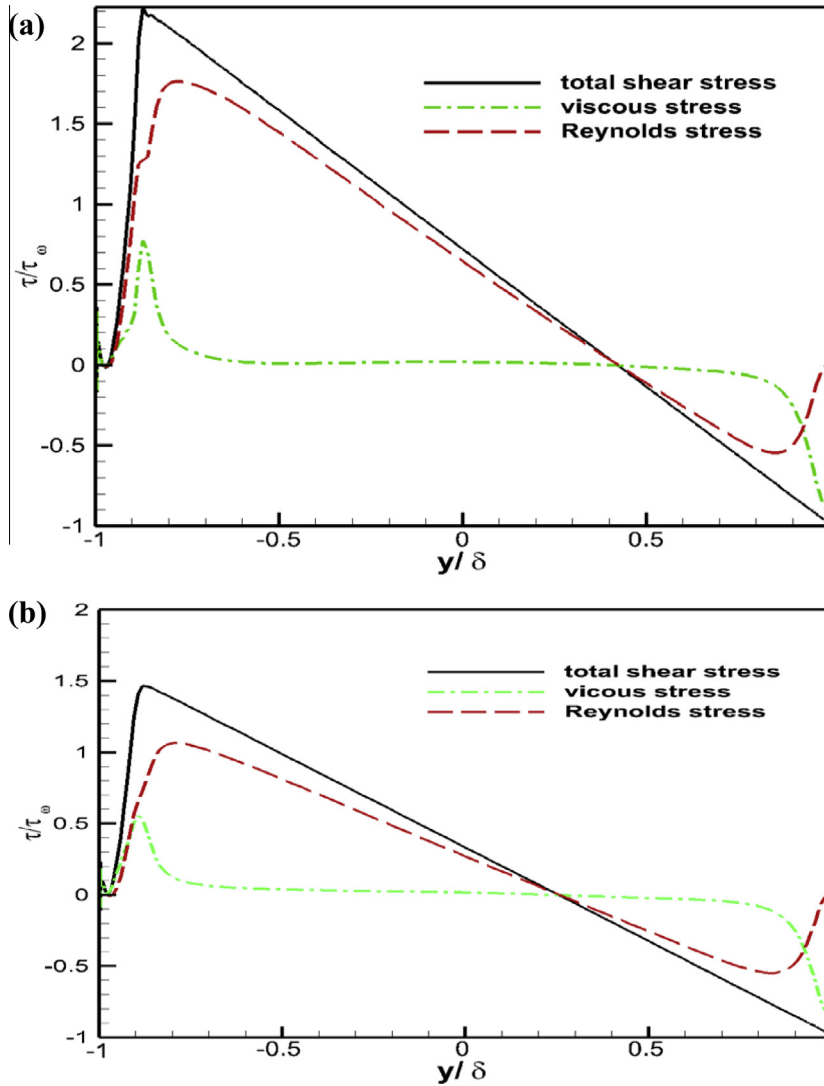


Fig. 9. Shear stress profiles normalized by upper wall shear stress; (a) ideal roughness,  $\lambda/h = 9$ ; (b) irregular roughness  $\lambda/h_{\max} = 9$ .

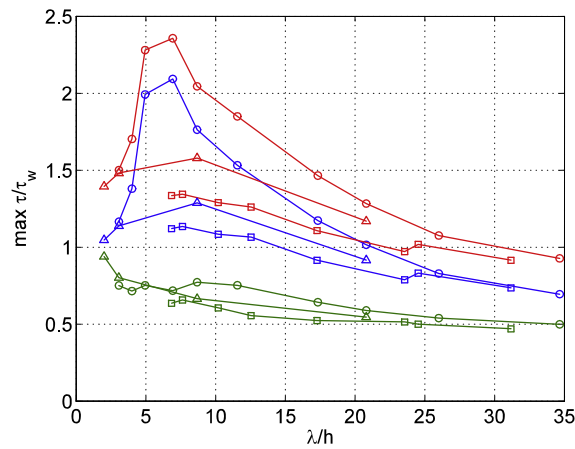
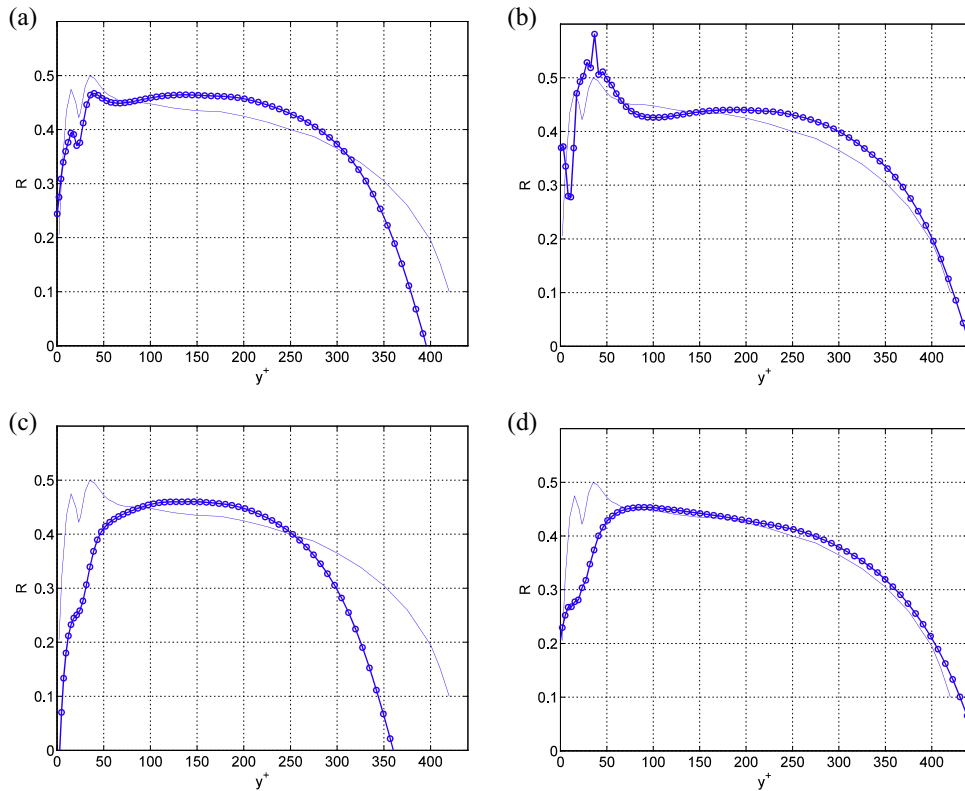


Fig. 10. Maximum values of shear stress components normalized by upper wall shear stress for all cases. — Total shear stress, — Reynolds stress, — viscous stress  $\square$  - irregular,  $\circ$  - 3-D ideal,  $\triangle$  - 2-D ideal.



**Fig. 11.** Correlation coefficient of Reynolds shear stress: (a) irregular,  $\lambda/h_{\max} = 4$ ; (b) 3-D ideal,  $\lambda/h = 4$ ; (c) random,  $\lambda/h_{\max} = 12$ ; (d) 3-D ideal,  $\lambda/h = 12$ .  $\circ$  this study; — DNS, data from [26] [37].

Reynolds stress, and viscous stress for all cases are plotted versus  $\lambda/h$  in Fig. 10. It is clear that viscous stresses were not significantly affected by the roughness distribution. For any given  $\lambda/h$ , the peak viscous values were comparable to each other, with the largest difference seen for  $10 < \lambda/h < 15$ , where the values were still within approximately 30% of each other. However, while total shear stress and Reynolds stress were reduced at small  $\lambda/h$ , viscous stress was seen to increase. This was expected, as Leonardi et al. Bhaganagar and Juttijudata [15] showed that viscous drag is dominant at very small  $\lambda/h$  (e.g.  $\lambda/h = 1$ ) and suggested that the ratio of viscous drag to form drag be used as the true indicator of whether a flow should be classified as  $k$ - or  $d$ -type. Reynolds and total shear stress were seen to be maximized at  $\lambda/h = 7$  for the ideal cases (2-D case based on polynomial interpolation, not shown), with 3-D roughness clearly increasing the stress, especially for  $4 < \lambda/h < 17$ .

We consider the correlation coefficient of the Reynolds stress which is defined as,

$$\mathbf{R} = \frac{-\overline{\mathbf{u}^T \mathbf{v}'}}{\mathbf{u}_{\text{rms}} \nu_{\text{rms}}}. \quad (4)$$

$R$  is shown for various cases in Fig. 11. The data is compared to the DNS study of Singh et al. of flow over a rough bed composed of densely packed spheres (2007). Irregular roughness cases for  $\lambda/h_{\max} < 7$  exhibited two peaks similar to what is seen in Fig. 11(a). As  $\lambda/h_{\max}$  increases, the peaks were seen to dissipate and the distribution gradually changed into what is seen in Fig. 11(c), which exhibits no near-wall peak. Surprisingly, irregular-roughness cases at small  $\lambda/h_{\max}$  were the only cases which exhibited two peaks similar to what was seen by Singh et al.

Idealized roughness cases only exhibited one sharp peak for  $\lambda/h < 5$  (Fig. 11(b)). The correlation coefficient for flow over a smooth wall is qualitatively similar to Fig. 11(b), except with a softer near-wall peak with a maximum of approximately 0.45.

#### 4. Conclusions and discussion

Direct numerical simulations of a turbulent channel flow at low Reynolds number of  $Re_\tau$  of 180 for flow over rough wall with idealized and irregular, 3-D roughness has been conducted.

The roughness geometries have been generalized such that roughness shape, density and height are similar for both the idealized and irregular roughness. In this present work, we conduct a systematic work on the role of  $\lambda/h$  parameter in altering the mean and turbulence fields over a rough wall for both idealized and irregular roughness. We focus on the mean and turbulence flow statistics in order to understand the differences in the flow over the rough walls with idealized and irregular

roughness. The simulations were performed for ten idealized roughness cases and eight irregular roughness cases with mean streamwise spacing of roughness  $\lambda/h$  varying from 3 to 35. The results have revealed that the flow over idealized and irregular roughness responds differently.

Surface roughness produces an expected downward shift of the mean velocity in  $U^+$ . For the idealized roughness with closely spaced roughness ( $\lambda/h < 9$ ), the shift increases with increasing  $\lambda/h$ , and the trend is reversed for sparsely packed roughness. For the irregular roughness, the downward shift of  $U^+$  is independent of  $\lambda/h$ . It is known that the increased downward shift of  $U^+$  corresponds to an increase of drag coefficient; it suggests that drag coefficient is strong function of  $\lambda/h$  for regular roughness and it is almost insensitive to  $\lambda/h$  for irregular roughness. The presence of two distinct behaviors for regular roughness can be explained using the concept of solidity factor, a measure of degree of sparseness introduced by Schlichting [20] and later modified by Sigal and Danberg [21].

The solidity scaling is reasonable from the first principles, a simple scaling analysis of the mean momentum equations yields that the drag force per unit area in the streamwise direction ( $F_{dx}$ ) is directly proportional to the pressure drop times the solidity ( $\lambda_s$ ), as follows:

$$F_{dx} \sim \frac{1}{L_x L_z} \int \int \int_{vol} P n_x \delta(x - x_s) dV \sim \Delta P \frac{1}{L_x L_z} \int \int \int_{vol} |n_x| \delta(x - x_s) dV \sim \Delta P \times \frac{A_f}{L_x L_z} \sim \Delta P \lambda_s, \quad (5)$$

where,  $\Delta P$  is the pressure drop across a roughness element,  $A_f$  is the frontal cross-sectional area of the roughness element,  $L_x$  and  $L_z$  is the length of the domain in  $x$ - and  $z$ -directions respectively. For low solidity (which corresponds to large sparseness), decreasing the spacing between the elements increases the drag until a maximum is reached. Further, decrease in the spacing leads to larger solidity (lower sparseness) and decreased drag. The present DNS has clearly demonstrated that for idealized 3D ripple shaped roughness,  $\lambda/h$  in the range of 7–9 is a transition range for the two distinct behaviors.

On comparing the turbulent intensities, it is clear that regular and irregular roughness distributions exhibit significant differences. The turbulence intensities for irregular roughness are insensitive to  $\lambda/h$ . The roughness geometries considered have same root-mean-square of height, positive skewness in the range of 0.28–0.67 and kurtosis in the range of 1.79–2.2. For all the cases considered, it is clear that though the spacing is varied for different cases, the peakedness and effective roughness height (root-mean-square of height) is similar for all these cases. For both the regular and irregular roughness, the effect of roughness is confined only to the inner layer for the mean velocity profile, thus demonstrating no inner/outer layer interactions for the mean flow.

The peak turbulence intensities over regular and irregular roughness are higher compared to the smooth wall. For idealized roughness, the effect of the spacing is also present in the outer layer as seen from turbulence intensities. For low solidity, decreasing the spacing between the elements influences the effect of the roughness to a larger vertical extent until it reaches a maximum, as seen from the shift of the location of minimum  $u_{rms}$ . The location of the peak  $u_{rms}$  scaled with rough wall  $u_\tau$  moves towards the wall with increasing  $\lambda/h$  for large solidity suggesting enhanced turbulence production attaining a maximum at  $\lambda/h = 9$ . For irregular roughness, no inner/outer layers interactions were observed. The irregular roughness alters the flow only in the inner layer, and the differences due to the roughness spacing are present in the near-wall region. The large scale structures as revealed from the turbulence intensities are significantly different between the idealized and irregular roughness.

For idealized roughness  $\lambda/h$  is valid measure to parameterize the large scale features of the flow for 3-D ripple shaped roughness elements. On the other hand, it is clear that statistical parameters to quantify irregularity such as skewness, kurtosis or rms of height are required. It is likely that though  $\lambda/h$  varies substantially for the cases considered, as the skewness and kurtosis vary in the narrow margin of 0.28–0.67 and 1.79–2.2, no significant effect of roughness on the outer layer are present.

Summarizing the state of art of rough-wall research, there is enough experimental evidence that reinforce the outer layer similarity hypothesis; however, there is also substantial evidence that rough surfaces can be very different from the smooth surfaces throughout the boundary layer, which clearly conflict the Townsend's boundary layer hypothesis. Efforts have been directed in addressing inner/outer layer controversy including the works of Jimenez who suggested that scale separation between the roughness height ( $h$ ) and the boundary layer thickness ( $d$ ) of  $d/h > 40$  is required for roughness to perturb the surface boundary conditions; however, the recent experiments of [22] have demonstrated rough surface consisting of spanwise square bars exhibited outer-layer similarity for  $d/h = 130$ . Efforts have been directed in classifying the inner/outer effects based on roughness geometrical parameters. The importance of the density of roughness elements was suggested by Colebrook and White [23] and shown in recent works e.g. Sigal and Danberg [21], Shockling et al. [24]. Leonardi et al. [25] relate the transition between  $k$ - and  $d$ -type of rough walls [1] to the relative contribution of friction drag and form drag.

In light of the full range of experimental/numerical results, it now appears that rough-wall boundary layers can be categorized according to whether or not the surface roughness affects the outer layer (although to some extent this classification will depend on which statistic is examined). Placing the present work in the perspective of the above research, we can now clearly demonstrate that given the shape and height of roughness, for the idealized roughness, the mean flow and turbulence fluctuations can be characterized in terms of  $\lambda/h$  and the solidity ratio (densely or sparsely spaced roughness). The extent of modification in the outer-layer is dictated primarily by the length scales that originate due to roughness. On the other hand, that the length scales corresponding to roughness element are irrelevant for irregular roughness. For the same roughness height and roughness shape, there is no inner/outer interaction for irregular roughness, but significant inner/outer interaction for regular roughness. Further, that flow over irregular rough wall does not see any differences

between closely packed and sparsely packed roughness elements. The study is a success as it answers one of the important controversies in the rough-wall research on the fundamental differences between the idealized and irregular roughness. It also successfully categorizes the idealized rough wall based on the solidity ratio (degree of sparseness). It clearly demonstrates that irregular roughness cannot be categorized based on roughness length scales, but suggests skewness, kurtosis and other statistical parameters of roughness height to be better metrics. The results further indicate need for significant future experimental and numerical work to be performed for irregular roughness with varied skewness (positive and negative) and kurtosis parameters to quantify the effect the roughness on turbulence.

## References

- [1] A.E. Perry, W.H. Schofield, P.N. Joubert, Rough wall turbulent boundary layers, *J. Fluid Mech.* 37 (1969) 383–413.
- [2] I. Tani, Turbulent boundary layer development over rough surfaces, in: H.U. Meier, P. Bradshaw (Eds.), *Perspectives in Turbulence Studies*, Springer-Verlag, Berlin, 1987, pp. 223–249.
- [3] P.A. Krogstad, R. Antonia, Surface roughness effects in turbulent boundary layers, *Exp. Fluids* 27 (1999) 450–460.
- [4] S. Leonardi, P. Orlandi, R.J. Smalley, L. Djenidi, R.A. Antonia, Direct numerical simulations of turbulent channel flow with transverse square bars, *J. Fluid Mech.* 491 (2003) 229–238.
- [5] L. Djenidi, R. Elavarasan, R.A. Antonia, Turbulent boundary layer over transverse square cavities, in: *13th Australasian Fluid Mechanics Conference*, December 1998, pp. 837–840.
- [6] P. Orlandi, S. Leonardi, DNS of 3D turbulent rough channels: parameterization and flow physics, *J. Fluid Mech.* 606 (2008) 399–415.
- [7] J. Cui, V.C. Patel, C.-L. Lin, Large-eddy simulation of turbulent flow in a channel with rib roughness, *Int. J. Heat Fluid Flow* 24 (2003) 372–388.
- [8] Napoli, E. Armenio, M. Marchis, The effect of the slope of irregularly distributed roughness elements on turbulent wall-bounded flows, *J. Fluid Mech.* 613 (2008) 385–394.
- [9] K. Flack, M. Schultz, Review of hydraulic roughness scales in the fully rough regime, *J. Fluid Eng.* 132 (2010).
- [10] C.S. Subramanian, P.I. King, M.F. Reeder, Effects of strong irregular roughness on the turbulent boundary layer, *Flow Turbul. Combust.* 72 (2004) 349–368.
- [11] K. Bhaganagar, J. Kim, G. Coleman, Effect of roughness on wall-bounded turbulence, *Flow Turbul. Combust.* 72 (2004) 463–492.
- [12] K. Bhaganagar, Direct numerical simulation of unsteady flow in channel with rough walls, *Phys. Fluids* 20 (10) (2008).
- [13] K. Bhaganagar, Direct numerical simulation of flow in stenotic channel to understand the effect of stenotic morphology on turbulence, *J. Turbul.* 10 (2009) 1080.
- [14] K. Bhaganagar, T.-J. Hsu, Direct numerical simulations of flow over two-dimensional ripples and implication to sediment transport: steady flow, *Coastal Eng.* 56 (3) (2009) 320–331.
- [15] K. Bhaganagar, V. Juttijudata, Understanding flow over rough-wall using proper orthogonal decomposition, *Theoret. Comput. Fluid Dyn.* 26 (6) (2011) 583–589, <http://dx.doi.org/10.1007/s00162-011-0242-x>.
- [16] K. Bhaganagar, D. Rempfer, J. Lumley, Direct numerical simulation of Spatial transition to turbulence using fourth-order vertical velocity second order vertical vorticity formulation, *J. Comp. Phys.* 180 (1) (2002) 200–228.
- [17] M.J. Yusof, Combined immersed-boundary/B-spline methods for simulations of flow in complex geometries. CTR-Annual Research Briefs – Stanford Univ./NASA Ames, 1997.
- [18] R.A. Bagnold. *The Physics of Blown Sand and Desert Dunes*, Methuen, 1941
- [19] L. Chau, K. Bhaganagar, Understanding turbulent flow over ripple-shaped random roughness in a channel, *Phys. Fluids* 24 (11) (2012). 115102–115102-22.
- [20] H. Schlichting, Experimental investigation of the problem of surface roughness, NACA Technical Memorandum 823, 1937.
- [21] A. Sigal, J.E. Danberg, New correlation of roughness density effect on the turbulent boundary layer, *AIAA J.* 28 (1990) 554–556.
- [22] P.A. Krogstad, V. Efron, About turbulence statistics in the outer part of a boundary layer developing over two-dimensional surface roughness, *Phys. Fluids* 24 (7) (2012).
- [23] C.F. Colebrook, C.M. White, Experiments with fluid friction in roughened pipes, *Proc. R. Soc. Lond.* 161 (1937) 367–381.
- [24] M.A. Shockling, J.J. Allen, A.J. Smits, Roughness effects in turbulent pipe flow, *J. Fluid Mech.* 564 (2006) 267–285.
- [25] S. Leonardi, P. Orlandi, R.A. Antonia, Properties of d- and k-type roughness in a turbulent channel flow, *Phys. Fluids* 19 (2007).
- [26] K.M. Singh, N.D. Sandham, J.J.R. Williams, Numerical simulation of flow over a rough bed, *J. Hydraulic Eng.* 386–398 (2007).